EARTHQUAKES

Casting stress shadows

Earthquakes may trigger or retard quakes on nearby faults, but such relationships are difficult to verify. Observations showing that the Landers earthquake in California shut down aftershocks from a preceding event validate such relationships.

Andrew M. Freed

The relentless build-up of stress associated with the motion of Earth's tectonic plates causes earthquakes. Communication of stress between faults, however, may also play an important role in earthquake triggering. How this stress communication occurs, and whether it significantly impacts earthquake occurrence, has long been a subject of debate. Earthquakes cause two types of stress: small but permanent — static — stress changes[1] in the surrounding crust due to fault slip, and large but temporary — dynamic— stress changes[2] due to the passage of seismic waves. Either of these mechanisms could be responsible for the triggering of aftershocks. Writing in *Nature Geoscience*, Toda *et al.*[3] analysed aftershocks following two earthquakes that occurred only two months apart, to show that static stress changes play a critical role in inducing aftershocks and, by extension, in triggering earthquakes in general.

Earthquakes tend to occur in clusters, where seismically active regions toggle between years of vigorous activity and periods of relative quiescence. Sumatra, for example, has experienced great ($M \geq 8$) earthquakes in 2004, 2005, 2007 and April 2012. Yet, before 2004, the last great quakes in this region occurred more than 150 years ago[4]. As another example, fourteen $M \geq 6$ earthquakes occurred in the 75 years before the 1906 San Francisco earthquake, but only one earthquake of such magnitude occurred in this region in the following 75 years[5]. Such clustering implies that faults communicate with each other through static

stress changes in the surrounding crust following earthquakes. Static stress changes are thought to be a key factor in earthquake clustering because these changes will be positive in certain regions, encouraging neighbouring faults to rupture[2], and negative in other regions (known as stress shadows), causing faults in these areas to stay quiet. Because static stress changes are permanent, they can bring a neighbouring fault closer to failure, even if it takes many more years of plate motions to actually induce the earthquake. In contrast, dynamic stress changes from seismic shaking are not thought to discourage earthquake occurrence, and thus do not create stress shadows. Furthermore, because dynamic stress changes are not permanent, ceasing when shaking stops, this mechanism is not likely to influence earthquake occurrence years later.

Although the importance of static stress changes is assumed in prevalent theories for earthquake clustering, it is difficult to demonstrate that small changes in static stress can have a significant influence. To better understand this potential relationship, geophysicists have turned to studying aftershocks, the most easily observed form of earthquake triggering. Most aftershocks occur close to the earthquake mainshock, at distances less than the length of fault rupture, where static stress changes are significant. Furthermore, the pattern of aftershocks can be shown to approximately correspond to regions where static stress changes are calculated to encourage and discourage aftershocks[6]. However, dynamic triggering may also be responsible for the triggering of aftershocks, as they are often observed to be denser where seismic shaking is greatest[7]: beyond the edge of the fault, towards the direction in which rupture propagated. The aftershocks occur due to an accumulation of seismic energy in this region. Furthermore, aftershocks can be triggered over distances longer than several fault lengths from the earthquake epicentre[8], where static stress changes are insignificant. The relative importance of dynamic versus static stress changes for aftershock triggering has therefore remained controversial.

A discriminating test comes down to whether or not stress shadows exist, as they can only be induced by static stress changes. It is not enough to observe a paucity of aftershocks in regions where static stress drops are calculated to inhibit aftershocks; one must show that the rate of aftershocks in those regions has dropped from pre-earthquake seismicity rates. This has proved difficult to demonstrate, as seismicity in most regions is fairly quiet to begin with.

© MICHAEL RYMER / USGS

Figure 1 | Surface rupture created during the 1992 Landers earthquake, Mojave Desert, California. Toda *et al.*[3] show that aftershocks triggered by the 1992 *M* 6.1 Joshua Tree earthquake were shut off two months later by a reduction in static stress caused by the nearby *M* 7.3 Landers earthquake. The finding implies that static stress changes play an important role in aftershock occurrence and, by extension, may also affect earthquake clustering.

Toda *et al.*[3] therefore use observations from two earthquakes in southern California that were closely spaced in location and time to assess the role of static stress changes in earthquake triggering. The first earthquake, the *M* 6.1 Joshua Tree earthquake in 1992, generated vigorous aftershock activity that provided a background rate against which to measure any changes following the second earthquake. When the second, *M* 7.3 Landers earthquake struck two months later (Fig. 1), the aftershock activity from the first quake virtually stopped in areas that experienced a reduction in static stress from the Landers quake. Toda *et al.* clearly demonstrate that the Landers earthquake cast a stress shadow, therefore verifying their existence and, by extension, validating the role that static stress changes play in earthquake clustering.

The study does not negate the role that dynamic triggering must play in generating at least some aftershocks. Indeed, there seemed to be a short delay in the cessation of Joshua Tree aftershocks following the Landers quake. It could be that passing seismic waves, generating aftershocks as they travelled through the crust in the immediate aftermath of the Landers quake, temporarily masked the signal of reduced static stress and the stress shadow.

Static stress changes themselves, however, provide no mechanism to explain observations of a time delay between earthquakes and aftershocks, or the time delay between sequences of earthquakes. Thus, calculating static stress changes can help us define where an earthquake is likely to strike next, but not when.

Nevertheless, the implication is that we can use past earthquakes to help improve our forecasting of future events by mapping changes in static stress changes. This includes an ability to forecast where aftershocks are most likely to occur following large earthquakes, as well as where earthquakes are likely to strike next in a sequence of large events. The latter can be accomplished by calculating stress changes caused by an earthquake, identifying which active faults or fault segments in the region are encouraged by the stress changes, and identifying from historical records which of those are late in their earthquake cycle and therefore likely to break in the medium-term future. It is these faults that are most susceptible to a nudge by their neighbours. Such information can then be included in probabilistic seismic hazard maps, such as those produced by the US Geological Survey[9].

The findings by Toda *et al.*[3] are a far cry from actual earthquake prediction. To be able to predict when an earthquake will occur, one would also have to know the state of stress on a fault, as well as the critical stress level that would trigger an earthquake. At present, we have virtually no means of measuring either factor. Even so, the study represents progress towards understanding the very complex and chaotic process of earthquake clustering. If we can forecast where earthquakes are likely to occur, we can prepare for and hopefully mitigate the damage. ❐

Andrew M. Freed is at the Department of Earth, Atmospheric and Planetary Sciences, Purdue University, 550 Stadium Mall Drive, West Lafayette, Indiana 47907, USA.
e-mail: freed@purdue.edu

References

1. Stein, R. S. *Nature* **402,** 605–609 (1999).
2. Kilb, D., Gomberg, J. & Bodin, P. *Nature* **408,** 570–574 (2000).
3. Toda, S., Stein, R. S., Beroza, G. C. & Marsan, D. *Nature Geosci.* **5,** 410–413 (2012).
4. Natawidjaja, D. H. *et al. J. Geophys. Res.* **111,** B06403, (2006).
5. Bakun, W. H. *Bull. Seismol. Soc. Am.* **89,** 764–784 (1999).
6. King, G. C. P., Stein, R. S. & Lin, J. *Bull. Seismol. Soc. Am.* **84,** 935–93 (1994).
7. Gomberg, J., Bodin, P. & Reasenberg, P. A. *Bull. Seismol. Soc. Am.* **93,** 118–38 (2003).
8. Hill, D. P., Reasenberg, P. A., Michael, A. J., Arabasz, W. J. & Beroza, G. C. *Science* **260,** 1617–1623 (1993).
9. http://earthquake.usgs.gov/hazards/

nature geoscience

LETTERS

PUBLISHED ONLINE: 6 MAY 2012 | DOI: 10.1038/NGEO1465

Aftershocks halted by static stress shadows

Shinji Toda[1]*, Ross S. Stein[2], Gregory C. Beroza[3] and David Marsan[4]

Earthquakes impart static and dynamic stress changes to the surrounding crust. Sudden fault slip causes small but permanent—static—stress changes, and passing seismic waves cause large, but brief and oscillatory—dynamic—stress changes. Because both static and dynamic stresses can trigger earthquakes within several rupture dimensions of a mainshock, it has proven difficult to disentangle their contributions to the triggering process[1–3]. However, only dynamic stress can trigger earthquakes far from the source[4,5], and only static stress can create stress shadows, where the stress and thus the seismicity rate in the shadow area drops following an earthquake[6–9]. Here we calculate the stress imparted by the magnitude 6.1 Joshua Tree and nearby magnitude 7.3 Landers earthquakes that occurred in California in April and June 1992, respectively, and measure seismicity through time. We show that, where the aftershock zone of the first earthquake was subjected to a static stress increase from the second, the seismicity rate jumped. In contrast, where the aftershock zone of the first earthquake fell under the stress shadow of the second and static stress dropped, seismicity shut down. The arrest of seismicity implies that static stress is a requisite element of spatial clustering of large earthquakes and should be a constituent of hazard assessment.

The great 1857 and 1906 San Andreas earthquakes provided the first evidence that stress shadows generated by mainshocks might inhibit subsequent earthquakes[6,7]. Further studies found that seismicity rates declined for months to years in portions of the stress shadows of the 1983 moment magnitude $M_w = 6.7$ Coalinga, 1989 $M_w = 6.9$ Loma Prieta, 1992 $M_w = 7.3$ Landers, 1994 $M_w = 6.7$ Northridge, 1997 $M_w = 6.1$ Kagoshima, 1999 $M_w = 7.4$ Izmit and 1999 $M_w = 7.6$ Chi-Chi shocks[8,10,11], although in some cases there was a seismicity increase at the time of the mainshock, followed by a rate drop beginning days[12], weeks[10,11,13] or months[14] after the earthquake. Other studies contend that the seismicity rate does not drop in the stress shadows[1,15–17]. Analyses of large sets of global surface-wave magnitude $M \geq 7$ earthquakes[18] have indicated that $\geq$0.1 bar Coulomb or shear-stress shadows exert only subtle effects on seismicity, and so have not resolved the debate.

At the very least, the conditions under which we can search the seismicity-rate declines in stress shadows have proved to be restrictive. Although the net Coulomb stress change in the crust surrounding an earthquake is zero (Fig. 1a) because there is no energy added to the crust, the net seismicity rate should sharply increase (Fig. 1b). Therefore, when all seismicity within a fixed radial distance from an epicentre or fault is counted, there will be a net gain that obscures any rate drop in the shadows. Detecting rate declines near the fault rupture, where the shadow should be strongest, is hampered by unresolvable geometrical and slip irregularities along the rupture that can produce local stress increases. To measure the rate drop there must also be a high rate of seismicity before the region falls under a stress shadow. The most favourable condition for detection thus occurs when two large nearby but not adjacent mainshocks strike within a few months of each other in a dense seismic network, in which the first earthquake turns on seismicity and the second turns it off[9].

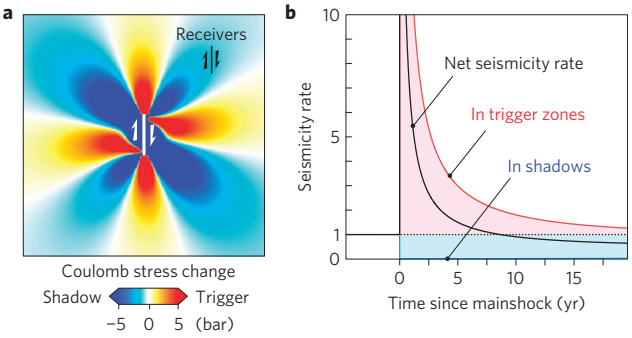

Figure 1 | The stress-trigger/stress-shadow imbalance. a,**b**, Even though there are equal volumes of stress increase and decrease associated with an earthquake (**a**), the resulting seismicity forecast by rate- and state-dependent friction[26] yields a sudden rate change followed by a recovery inversely proportional to time, resulting in a net gain in seismicity for times less than about 5 yr (**b**). Here we set the rate/state friction parameter multiplied by the normal stress, $A\sigma$, to 0.4 bar, and aftershock duration, t_a, to 10 yr, values appropriate for the Joshua Tree and Landers earthquakes. At times greater than t_a, the net seismicity rate becomes slightly negative.

These requirements are ideally fulfilled by the 23 April 1992 $M_w = 6.1$ Joshua Tree and 28 June 1992 $M_w = 7.3$ Landers earthquakes[19], whose rupture endpoints lie about 13 km apart (black and grey lines in Fig. 2a). The Joshua Tree[20] earthquake produced ~6,000 $M \geq 1.0$ aftershocks within a 20 km radius during the 66 days before the Landers quake struck (blue shocks in Fig. 2a). The four off-fault lobes of the Joshua Tree aftershocks evident in Fig. 1a are well explained by the Coulomb stress imparted by the main rupture[21]. The northern and eastern portions of the Joshua Tree aftershock zone largely shut down after Landers (the rate dropped by 96.5%; blue shocks uncovered by red shocks in Fig. 2a). The portions of the Joshua Tree aftershock zone that were subjected to a stress increase from the Landers earthquake (red stress lobes in Fig. 2b) underwent an abrupt seismicity-rate increase (Fig. 2c), whereas the portion of the aftershock zone that fell under Lander's stress shadow (blue stress lobes in Fig. 2b) shut down beginning 2–3 days later (Fig. 2d).

The Coulomb stress change depends on the source rupture model[22–25], and the geometry, rake and friction coefficient of the surrounding 'receiver' faults on which aftershocks occur. The stress lobes shown in Fig. 2, however, are only modestly different for four representative source models (Supplementary Fig. S1), and

[1]Disaster Prevention Research Institute, Kyoto University, Kyoto 611-0011, Japan, [2]US Geological Survey, Menlo Park, California 94025, USA, [3]Department of Geophysics, Stanford University, Stanford, California 94305, USA, [4]ISTerre, Université de Savoie, CNRS, 73376 Le Bourget du Lac, France.
*e-mail: toda@rcep.dpri.kyoto-u.ac.jp.

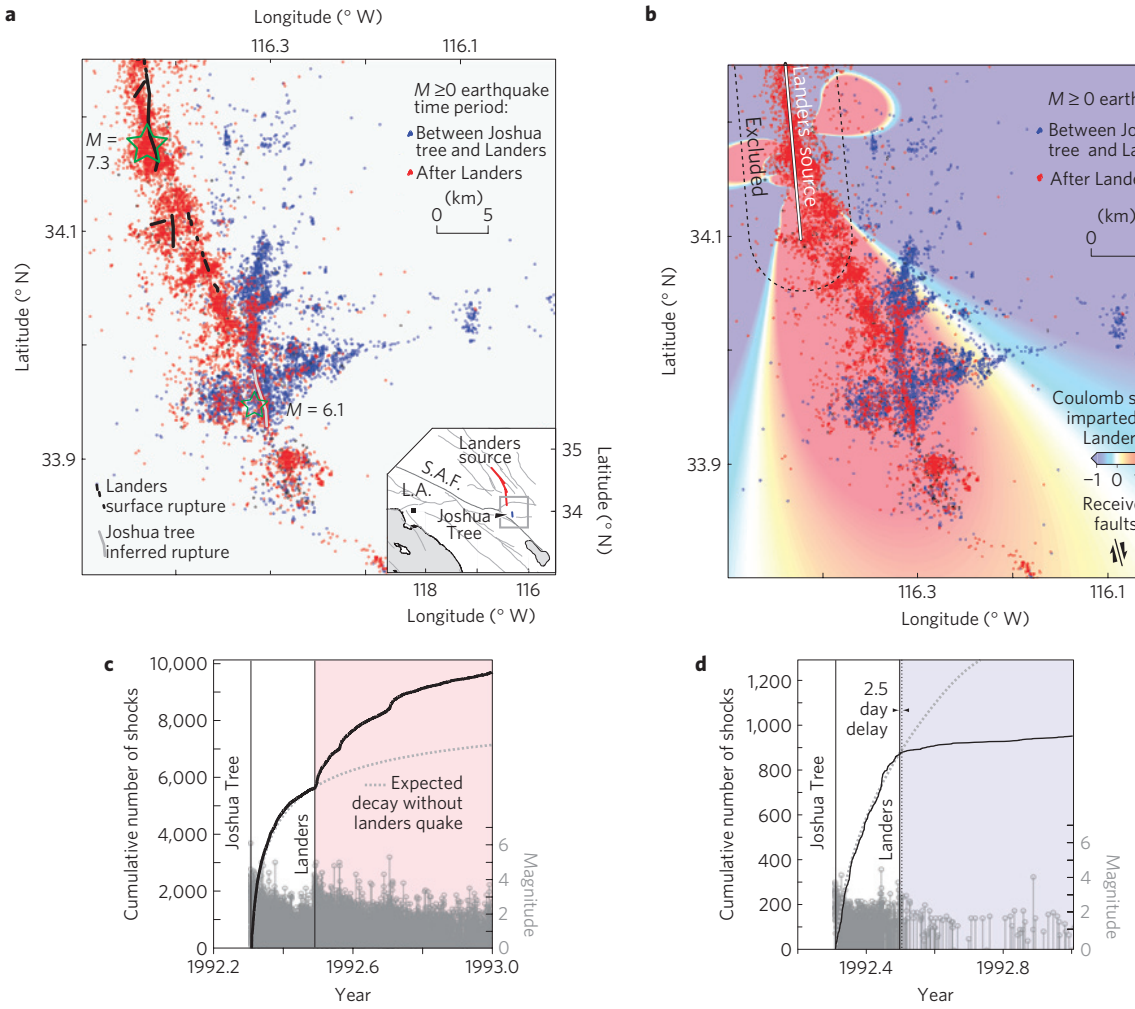

Figure 2 | Seismicity shutdown in the Landers stress shadow. a, Seismicity (SHKL, ref. 33, relocated catalogue without quarry blasts) associated with the 1992 Joshua Tree and Landers earthquakes. Earthquakes occurring during the 66 days between the Joshua Tree and Landers earthquakes are blue, and earthquakes from Landers to the end of 1992 (184 days) are red, revealing a shutdown within the stress shadow (blue region). The San Andreas Fault (S.A.F.) and Los Angeles (L.A.) are shown in the inset. **b**, Coulomb stress imparted by the Landers earthquake at 7.5 km depth for vertical right-lateral receiver faults striking 345° with friction of 0.4. **c**,**d**, Time series of earthquakes in the stress-trigger (**c**) and stress-shadow (**d**) zones. Earthquakes within 5 km of the Landers source (dashed line in **b**) are excluded because of source-model simplicity and uncertainty.

values of receiver fault friction (Supplementary Fig. S2). The most common Joshua Tree aftershocks are right lateral, followed by normal mechanisms (a full presentation of the mechanisms with ternary diagrams of their diversity is shown in Supplementary Fig. S3). Observed $M \geq 2$ earthquakes in the calculated stress shadows for both strike-slip and normal receivers declined after the Landers earthquake regardless of assumed friction (Supplementary Fig. S4). In Fig. 3, the stress imparted by the Landers earthquake[22] to the nodal planes of the focal mechanisms is shown, rather than that to a fixed receiver fault geometry as in Fig. 2. There is a mean 2 bar stress drop on the nodal planes, but with some planes being subjected to a stress increase (Fig. 3b). Because of mechanism uncertainty and because we do not know which nodal plane slipped, the histogram of the Fig. 3b inset is only a realization of the true distribution, but it is probably more realistic than using the single, dominant receiver plane for all shocks of Fig. 2b.

Is the seismicity-rate drop real? The rate drop cannot be attributed to a detection artefact, as the seismic network coverage was uniform across the Joshua Tree aftershock zone throughout 1992 (the station distribution is shown in Supplementary Fig. S5, and the magnitude of completeness as a function of time and space is shown in Supplementary Fig. S6). Further, because the shadow is located the same distance from the Landers rupture as the trigger zone, no detection bias favours the shadow, and both have the same seismic station density (Supplementary Fig. S5). The seismicity-rate decline is evident across all magnitude bands (Supplementary Fig. S7), and is clear even when the immediate post-mainshock periods are excluded. If detection rather than the seismicity rate had decreased, the rate decrease would have appeared in both trigger and shadow zones, which is not observed. We might ask if the shutdown is seen only because the Landers earthquake ruptured largely northward, away from Joshua Tree, resulting in negligible dynamic stress, but the peak dynamic stress at the site of the shutdown is calculated to be 45–60 bar[15], dwarfing the 2 bar static stress drop. Similar dynamic stress is calculated in the trigger zone[15], where the seismicity rate jumped. Finally, the seismicity-rate increase in the trigger zone makes it unlikely that the shutdown occurred because the Joshua Tree aftershocks had already expended the potential earthquake-nucleation sites.

Either a sudden or delayed shutdown can be explained by a rate/state friction implementation of Coulomb stress transfer[26]. Using the observed background seismicity rate, fitting for the aftershock duration, t_a, and a constitutive parameter multiplied by the normal stress, $A\sigma$, and using only the calculated stress decreases

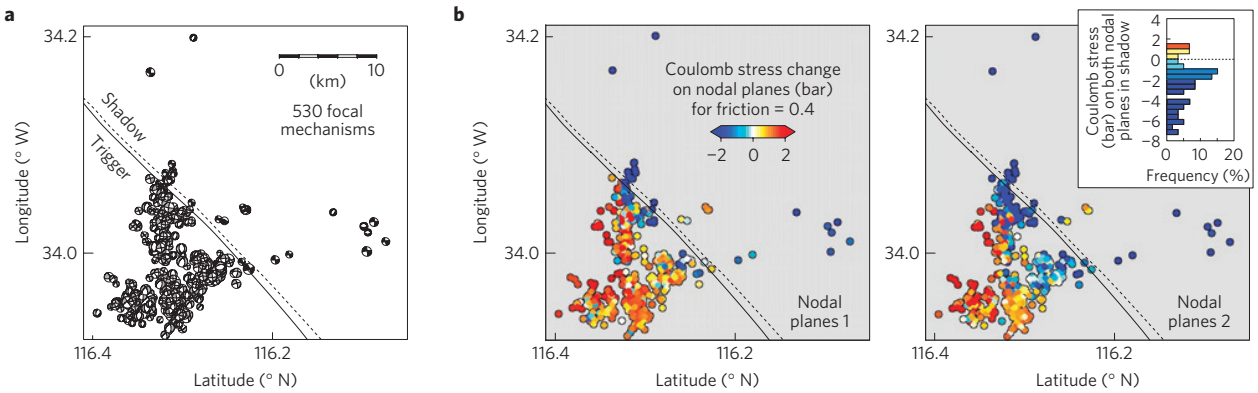

Figure 3 | Stress shadow imparted to the nodal planes of Joshua Tree aftershocks. a, Focal mechanisms for $M \geq 2.0$ events during the 66 days between the Joshua Tree[32] and Landers earthquakes. The black mechanisms lie within the stress shadow for strike-slip (dashed) and normal (solid) receiver faults. **b**, For non-zero fault friction, the Coulomb stress is different on the two planes, and so we calculate it on both planes using a standard Landers source model[22]. The stress decreases on most, but not all, mechanisms. Inset: histogram of Coulomb stress changes for both nodal planes within the stress shadow (northeast of the solid line).

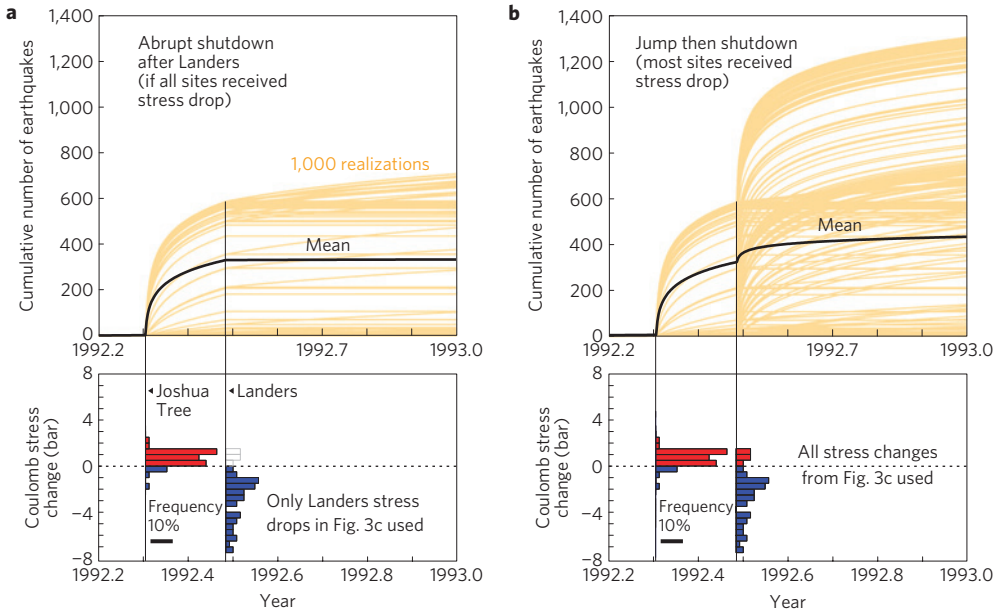

Figure 4 | Explanation of immediate and delayed rate drops in the stress shadow. Calculation of the expected number of Joshua Tree aftershocks in the Landers stress shadow. The Coulomb stress changes for the Joshua Tree and Landers earthquakes are drawn at random from the distribution shown in the lower panels. The seismicity-rate equation[26] is evolved for the Joshua Tree and Landers earthquakes in daily steps. The black curve is the mean of all 1,000 time histories (tan curves). **a**, When only the Landers stress decreases are used, the rate drop is immediate. **b**, When the full range of inferred stress changes imparted by Landers to the aftershock focal mechanisms is used, there is a rate jump and a delayed decline.

from Fig. 3c, a sudden shutdown of seismicity would have occurred (Fig. 4a). The same parameters can be employed to match the immediate seismicity-rate increase in the trigger zone, using the calculated stress increases to its aftershocks. However, when the full range of the calculated stress changes in Fig. 3c is used instead, a rate jump followed by a delayed shutdown occurs (Fig. 4b). This can explain the observed delay, as well as the one-day[9] to three-month[14] delay in the rate drop for other earthquakes (Methods). It is also possible that an immediate rate jump could be the product of dynamic stress triggering.

The more diverse the geometry of the faults surrounding the mainshock, the more likely there will be an immediate rate increase followed by a delayed decrease. Fault diversity most probably results from a low or heterogeneous regional tectonic stress[27,28]. Other sources of heterogeneity in the stress-change distribution can also delay the seismicity shutdown, including variations in crustal lithology or fluid pressure, the stress imparted by nearby aftershocks, or a recent change in the tectonic stress, none of which we consider. On the source fault itself, slip heterogeneity adds to this diversity, which may explain why delays are often observed in stress shadows along the fault rupture[26].

We have designed this study to overcome the shortcomings and limitations of our analysis of a seismicity-rate drop in the stress shadow of the 1997 Kagoshima, Japan, doublet[9]. First, several authors objected to the use of arbitrary boxes to search for rate drops[12,16]. Here, we define the sampled area by the stress changes themselves rather than by boxes, and the resulting seismicity-rate drop is observed over an area four times larger than at Kagoshima. A second criticism was that the seismicity-rate drop might instead be an artefact caused by degraded earthquake detection after the mainshock, or a change in background rate beforehand[12,16,19,29,30]. Here, we fully explore the network detection level and completeness

magnitude in time and space, and can exclude these possibilities. Third, some argued that, as seismicity-rate drops in stress shadows are commonly delayed, Kagoshima is exceptional rather than representative[29]. Here the shutdown delay is short, so there is little doubt that the Landers earthquake caused it, but long enough to be observable and thus part of a continuum that extends to longer delays. Finally, we consider that the Kagoshima study inadequately explored model uncertainty. Here we used four source models rather than one and three values of friction rather than two, and calculated the stress changes not only on the two dominant receiver planes but also on all aftershock nodal planes.

We thus find that stress shadows of large mainshocks can indeed halt aftershock occurrence, as required by the static Coulomb triggering hypothesis. The occurrence of a seismicity-rate drop in the stress shadow does not mean that dynamic triggering cannot also occur. Instead, we argue that static stress triggering must be one source of the production of aftershocks, and by extension subsequent mainshocks.

Methods

In Fig. 2b, the dominant strike of right-lateral receiver fault planes is determined from the 464 observed focal mechanisms within the stress shadow, calculated under the condition that the rake is within 10° of pure right lateral (Supplementary Fig. S4a). The same calculation is made for normal faults (Supplementary Fig. S4b), which comprise the next most common mechanism. The consequences of these assumptions, as well as those for the full range of possible fault friction (0.0–0.8), are shown in Supplementary Fig. S4c–f.

In Fig. 3, stress is calculated on both nodal planes of each mechanism at its hypocentre, rather than at a fixed depth as in Fig. 2b–d. We do not assume we know which nodal plane slipped, and so the stress changes on both planes are included in the histogram. Only if fault friction were zero would the Coulomb stress change have been the same on both planes.

In Fig. 4, the background seismicity rate in the stress shadow is set to 12 $M \geq 2.0$ earthquakes yr^{-1}, on the basis of the 1 January 1984–11 April 1992 catalogue. The distribution of Coulomb stress changes for the Joshua Tree and Landers earthquakes are simulated by 1,000 Monte Carlo draws from the distributions of Joshua stress changes. They are then evolved in one-day time steps until the time of the Landers earthquake, at which time they are modified by draws from the distributions of Landers stress changes, and again evolved in one-day time steps until 1993. The fitted rate and state friction parameters are $A\sigma = 0.1$ bar and $t_a = 10$ yr. This aftershock duration is similar to that for the 1992 $M_w = 6.1$ Big Bear aftershock sequence located at the same distance from the San Andreas fault[31] as Joshua Tree.

Received 23 August 2011; accepted 5 April 2012; published online 6 May 2012

References

1. Kilb, D., Gomberg, J. & Bodin, P. Earthquake triggering by dynamic stresses. *Nature* **408,** 570–574 (2000).
2. Freed, A. M. Earthquake triggering by static, dynamic, and postseismic stress transfer. *Annu. Rev. Earth Planet. Sci.* **33,** 335–367 (2005).
3. Hill, D. P. & Prejean, S. G. in *Treatise on Geophysics* Vol. 4 (ed. Kanamori, H.) 257–291 (Elsevier, 2007).
4. Gomberg, J. & Johnson, P. Dynamic triggering of earthquakes. *Nature* **437,** 830 (2005).
5. Velasco, A. A., Hernandez, S., Parsons, T. & Pankow, K. Global ubiquity of dynamic earthquake triggering. *Nature Geosci.* **1,** 375–379 (2008).
6. Jaumé, S. C. & Sykes, L. R. Evolution of moderate seismicity in the San Francisco Bay region, 1850 to 1993: Seismicity changes related to the occurrence of large and great earthquakes. *J. Geophys. Res.* **101,** 765–789 (1996).
7. Harris, R. A. & Simpson, R. W. In the shadow of 1857—the effect of the great Ft. Tejon earthquake on subsequent earthquakes in southern California. *Geophys. Res. Lett.* **23,** 229–232 (1996).
8. Stein, R. S. The role of stress transfer in earthquake occurrence. *Nature* **402,** 605–609 (1999).
9. Toda, S. & Stein, R. S. Toggling of seismicity by the 1997 Kagoshima earthquake couplet: A demonstration of time-dependent stress transfer. *J. Geophys. Res.* **109,** B02303 (2003).
10. Wyss, M. & Wiemer, S. The change in the probability for earthquakes in southern California due to the Landers Magnitude 7.3 earthquake. *Science* **290,** 1334–1338 (2000).
11. Toda, S. & Stein, R. S. Response of the San Andreas fault to the 1983 Coalinga–Nuñez Earthquakes: An application of interaction-based probabilities for Parkfield. *J. Geophys. Res.* **107,** 2126 (2002).
12. Woessner, J., Hauksson, E., Wiemer, S. & Neukomm, S. The 1997 Kagoshima (Japan) earthquake doublet: A quantitative analysis of aftershock rate changes. *Geophys. Res. Let.* **31,** L03605 (2004).
13. Daniel, G., Marsan, D. & Bouchon, M. Perturbation of the Izmit earthquake aftershock decaying activity following the 1992 M_w 7.2 Düzce, Turkey earthquake. *J. Geophys. Res.* **111,** B05310 (2006).
14. Ma, K-F., Chan, C-H. & Stein, R. S. Response of seismicity to Coulomb stress triggers and shadows of the 1999 $M_w = 7.6$ Chi-Chi, Taiwan, earthquake. *J. Geophys. Res.* **110,** B05S19 (2005).
15. Kilb, D. A strong correlation between induced peak dynamic Coulomb stress change from the 1992 M7.3 Landers, California, earthquake and the hypocenter of the 1999 M7.1 Hector Mine, California earthquake. *J. Geophys. Res.* **108,** 2012 (2003).
16. Felzer, K. R. & Brodsky, E. E. Testing the stress shadow hypothesis. *J. Geophys. Res.* **110,** B05S09 (2005).
17. Mallman, E. P. & Zoback, M. D. Assessing elastic Coulomb stress transfer models using seismicity rates in southern California and southwestern Japan. *J. Geophys. Res.* **112,** B03304 (2007).
18. Mallman, E. P. & Parsons, T. A Global search for stress shadows. *J. Geophys. Res.* **113,** B12304 (2008).
19. Marsan, D. & Nalbant, S. Methods for measuring seismicity rate changes: A review and a study of how the M_w 7.3 Landers earthquake affected the aftershock sequence of the M_w 6.1 Joshua Tree earthquake. *Pure Appl. Geophys.* **162,** 1151–1185 (2005).
20. Savage, J. C., Lisowski, M. & Murray, M. Deformation from 1973 through 1991 in the epicentral area of the 1992 Landers, California, earthquake ($M_s = 7.5$). *J. Geophys. Res.* **98,** 19951–919958 (1993).
21. King, G. C. P., Stein, R. S. & Lin, J. Static stress changes and the triggering of earthquakes. *Bull. Seismol. Soc. Am.* **84,** 935–953 (1994).
22. Wald, D. J. & Heaton, T. H. Spatial and temporal distribution of slip for the 1992 Landers, California earthquake. *Bull. Seismol. Soc. Am.* **84,** 668–691 (1994).
23. Cohee, B. P. & Beroza, G. C. Slip distribution of the 1992 Landers earthquake and its implications for earthquake source mechanics. *Bull. Seismol. Soc. Am.* **84,** 692–712 (1994).
24. Cotton, F. & Campillo, M. Frequency domain inversion of strong motions: Application to the 1992 Landers earthquake. *J. Geophys. Res.* **100,** 3961–3975 (1995).
25. Hernandez, B., Cotton, F. & Campillo, M. Contribution of radar interferometry to a two-step inversion of the kinematic process of the 1992 Landers earthquake. *J. Geophys. Res.* **104,** 13083–13099 (1999).
26. Dieterich, J. A constitutive law for rate of earthquake production and its application to earthquake clustering. *J. Geophys. Res.* **99,** 2601–2618 (1994).
27. Marsan, D. Triggering of seismicity at short timescales following Californian earthquakes. *J. Geophys. Res.* **108,** 2266 (2003).
28. Marsan, D. Can coseismic stress variability suppress seismicity shadows? Insights from a rate-and-state friction model. *J. Geophys. Res.* **111,** B06305 (2006).
29. Steacy, S., Gomberg, J. & Cocco, M. Introduction to special section: Stress transfer, earthquake triggering, and time-dependent seismic hazard. *J. Geophys. Res.* **110,** B05S01 (2005).
30. Cocco, M. *et al.* Sensitivity study of forecasted aftershock seismicity based on Coulomb stress calculation and rate- and state-dependent frictional response. *J Geophys. Res.* **115,** B05307 (2010).
31. Toda, S., Stein, R. S., Richards-Dinger, K. & Bozkurt, S. Forecasting the evolution of seismicity in southern California: Animations built on earthquake stress transfer. *J. Geophys. Res.* **110,** B05S16 (2005).
32. Hardebeck, J. L. & Shearer, P. M. Using S/P amplitude ratios to constrain the focal mechanisms of small earthquakes. *Bull. Seismol. Soc. Am.* **93,** 2434–2444 (2003).
33. Shearer, P., Hauksson, E. & Lin, G. Southern California hypocenter relocation with waveform cross-correlation, Part 2: Results using source-specific station terms and cluster analysis. *Bull. Seismol. Soc. Am.* **95,** 904–915 (2005).

Acknowledgements

We thank D. Kilb, A. Michael, T. Parsons, R. Harris and D. Schorlemmer for guidance and reviews.

Author contributions

All authors contributed to the ideas and tests pursued in the analysis. G.C.B. discovered the data set and its implications, S.T. designed and carried out most of the calculations, D.M. enhanced the statistical rigour and explained the delayed-shutdown phenomenon and R.S.S. wrote most of the text.

Additional information

The authors declare no competing financial interests. Supplementary information accompanies this paper on www.nature.com/naturegeoscience. Reprints and permissions information is available online at www.nature.com/reprints. Correspondence and requests for materials should be addressed to S.T.

nature geoscience

SUPPLEMENTARY INFORMATION

DOI: 10.1038/NGEO1465

Aftershocks halted by static stress shadows

Shinji Toda, Ross S. Stein, Gregory C. Beroza, and David Marsan

This section contains Supplementary Figures 1-7 and associated references

Supplementary Fig. S1. Dependence of the Landers stress shadow on the source model [22-25]. Here, stress is resolved on right-lateral receiver faults striking 345°, the dominant azimuth among the strike-slip mechanisms (Supplementary Fig. S4a-b). Calculated stress change is shown in the top panels, and the source model slip is shown in the lower panels. The Wald and Heaton (1994) model [22] is used in Figs. 2-4 and Fig. S2.

Supplementary Fig. S2. Dependence of the Landers stress shadow on fault friction, using Wald and Heaton (1994) model [22], resolved on to 345°-striking vertical right-lateral faults. The Coulomb components (**c**-**d**) are decomposed into shear (**a**) and unclamping (**b**) stress. Panel (**a**) corresponds to a receiver fault friction of 0.0.

Supplementary Fig. S3. Focal mechanisms colored by mechanism [31] for earthquakes centered on the 1992 Joshua Tree earthquake, separated by magnitude range and time period. The inset ternary Frohlich diagrams [33] give the distribution of mechanism type in each map. Mechanisms are distributed between pure strike-slip and pure normal, and there is no obvious mechanism change after the Landers mainshock.

Supplementary Fig. S4. Rose diagrams showing the range of azimuths for strike-slip (**a**) and normal (**b**) receiver faults, based on the focal mechanisms in Fig. S3 during the period between the Joshua Tree and the Landers earthquakes. Coulomb stress changes for strike-slip faults (**c**) and normal faults (**d**), calculated only where aftershocks occur. Grey circles are M≥2 earthquakes that struck between the Joshua Tree and Landers earthquakes, and magenta circles are for events after the Landers earthquake. (**e**) The cumulative number of earthquakes in the stress shadow for the dominant strike-slip receivers. (**f**) The cumulative number of earthquakes in the stress shadow for normal fault receivers. The zero stress change contour shifts slightly as a function of friction (**c**-**d**), altering the earthquake collection area for the cumulative plot. Irrespective of the values used, there is a near-complete seismicity shutdown (≥95% rate drop). This effect of receiver fault strike on the Landers stress-aftershock correlation was previously explored for a simpler case [34].

Supplementary Fig. S5. **a.** The 9 permanent and 17 portable seismic stations within 30 km of the Joshua Tree mainshock. Portable stations without code names or dates lack this bulletin information [35]. Aftershocks of the 8 Jul 1986 M=6.0 North Palm Springs earthquake surround station WRR. For some receiver fault orientations, the 1986 aftershock zone is also calculated to locate in the Landers stress shadow, but by 1992 the seismicity rate there was declining and so

low, at 20 M≥2 per year, that a rate drop cannot be confidently detected. **b**. Magnitude of completeness as a function of time in the dashed box that covers most of the central trigger and eastern shadow zones using [36].

Supplementary Fig. S6. Frequency-magnitude plots to determine the magnitude of completeness, Mc, and the Gutenberg-Richter *a* and *b* values using ZMAP [37], for the four off-fault lobes of Joshua Tree aftershocks, all roughly equidistant from the Joshua Tree source [20,38]. An Mc of 2.0 is consistent with the observations for the region of the stress shadow, lobes I and II.

Supplementary Fig. S7. The cumulative number of earthquakes in the stress shadow for various minimum magnitudes, assuming friction=0.4. (**a**) shows M≥0 to M≥2.0; (**b**) shows M≥2.5 to M≥3.0.

Supplementary References

[33] Frohlich, C. Triangle diagrams: ternary graphs to display similarity and diversity of earthquake focal mechanisms. *Phys. Earth and Planet. Int.* **75**, 193-198, doi:110.1016/0031-9201(1092)90130-N (1992).

[34] Kilb, D. & Hardebeck, J. L. Fault parameter constraints using relocated earthquakes: A validation of first motion focal mechanism data. *Bull. Seis. Soc. Am.* **96**, 1140-1158, doi: 1110.1785/0120040239 (2006).

[35] Wald, L. A., Watts, K., Mori, J. & Douglass, K. Southern california network bulletin, January-December 1992. *U.S. Geol. Open-File Rep. 93-227*, 52 (1993).

[36] Woessner, J. & Wiemer, S. Assessing the quality of earthquake catalogues: Estimating the magnitude of completeness and its uncertainty. *Bull. Seism. Soc. Am.* **95**, 684-698; DOI: 610.1785/0120040007 (2005).

[37] Wiemer, S. A software package to analyse seismicity: ZMAP. *Seismol. Res. Letts.* **72**, 373-382 (2001).

[38] Ammon, C. J., Velasco, A. A. & Lay, T. Rapid estimation of rupture directivity: Application to the 1992 Landers (Ms = 7.4) and Cape Mendocino (Ms = 7.2), California earthquakes. *Geophys. Res. Lett.* **20**, 97-100 (1993).

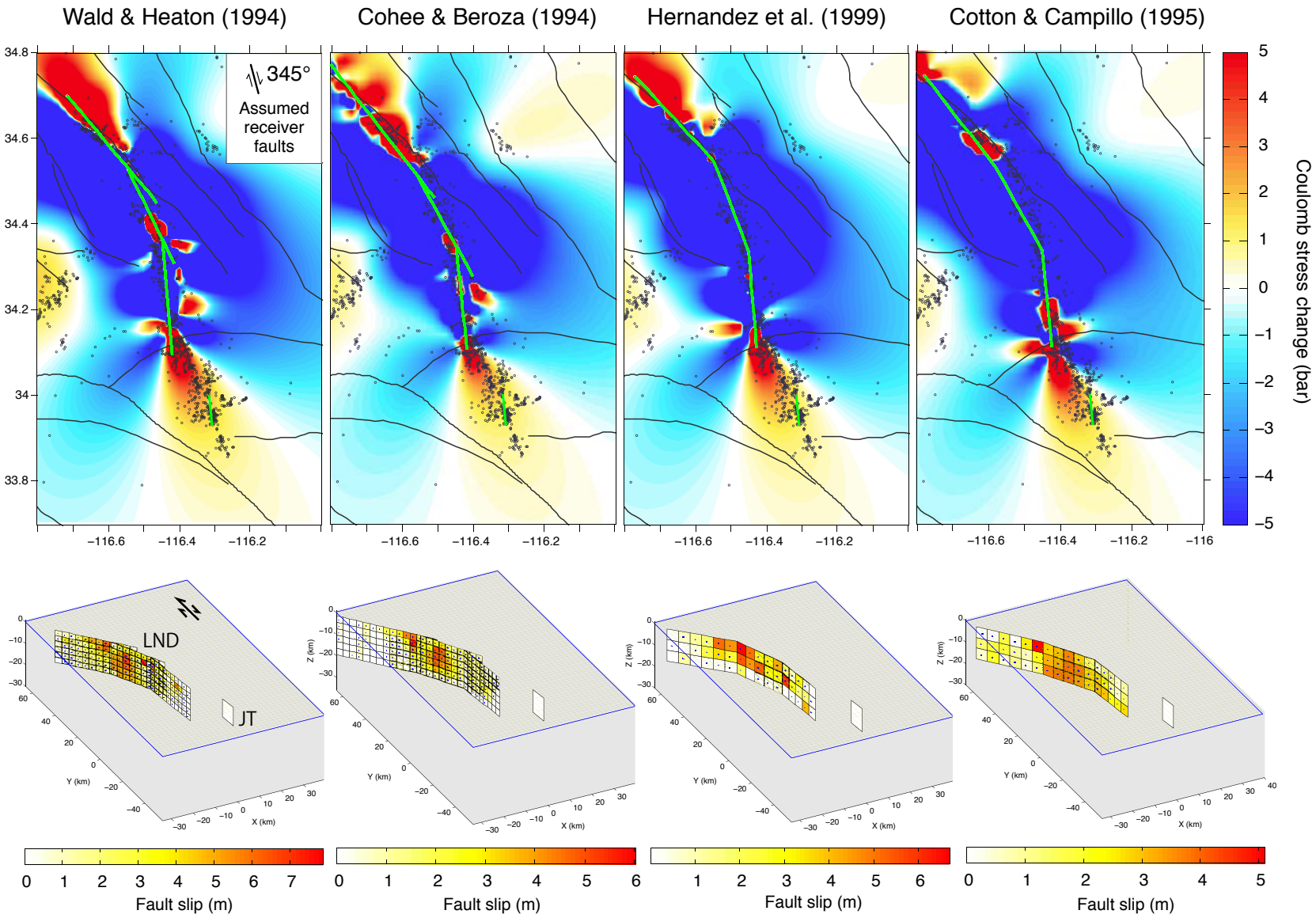

Supplementary Figure 1
NGS-2011-08-01314C
Toda et al.

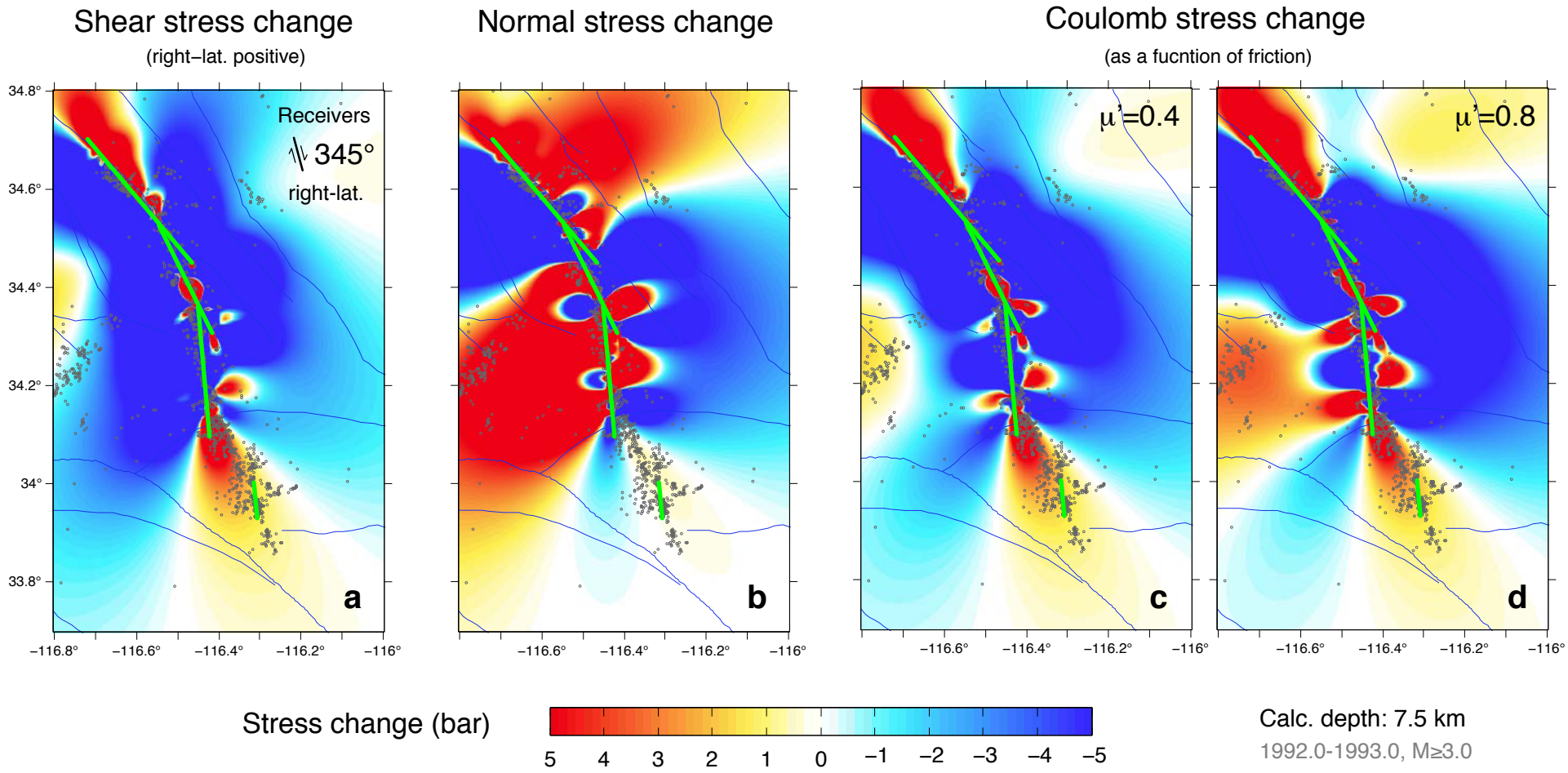

Supplementary Figure 2
NGS-2011-08-01314C
Toda et al.

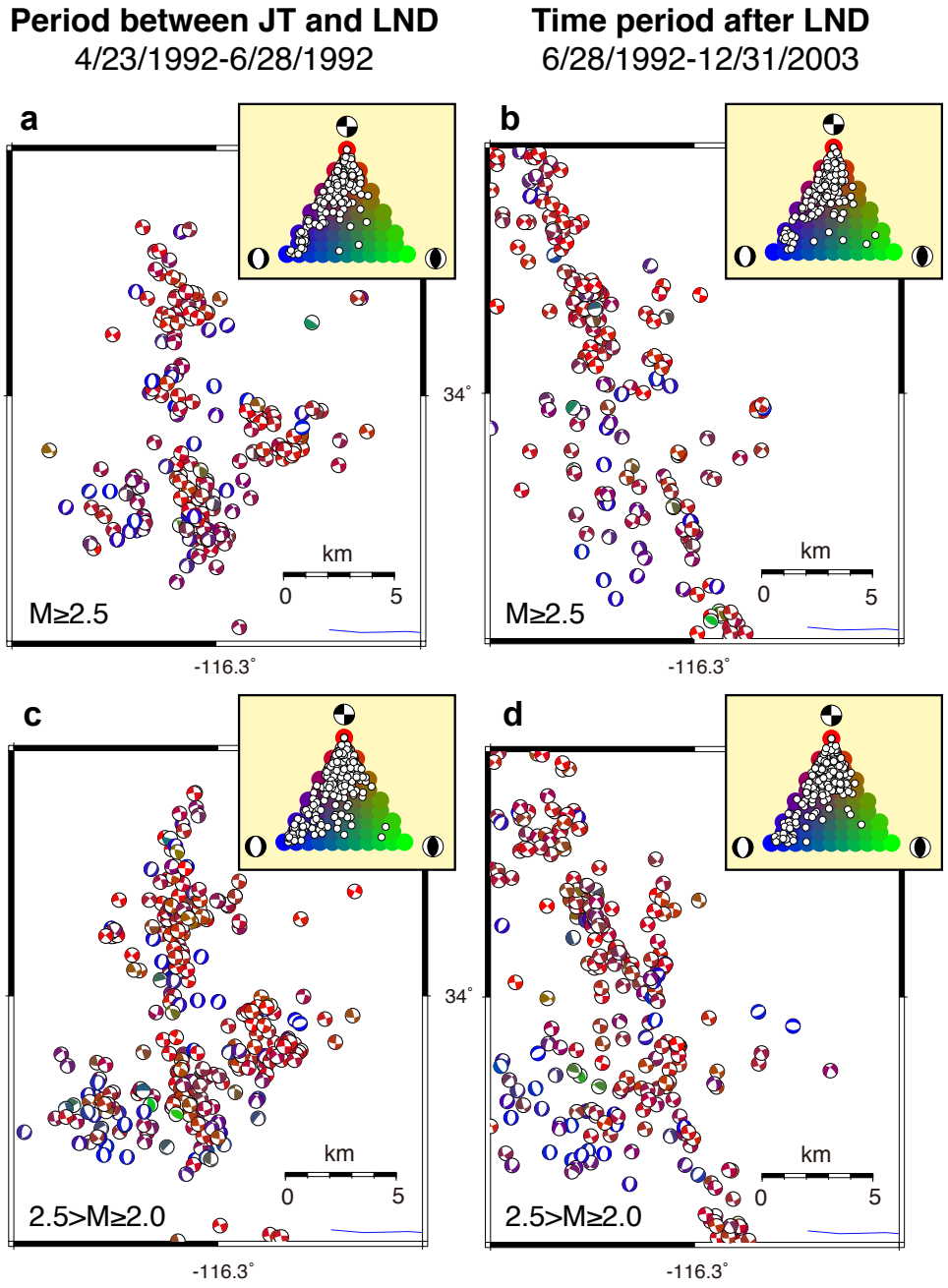

Supplementary Figure 3
NGS-2011-08-01314C
Toda et al.

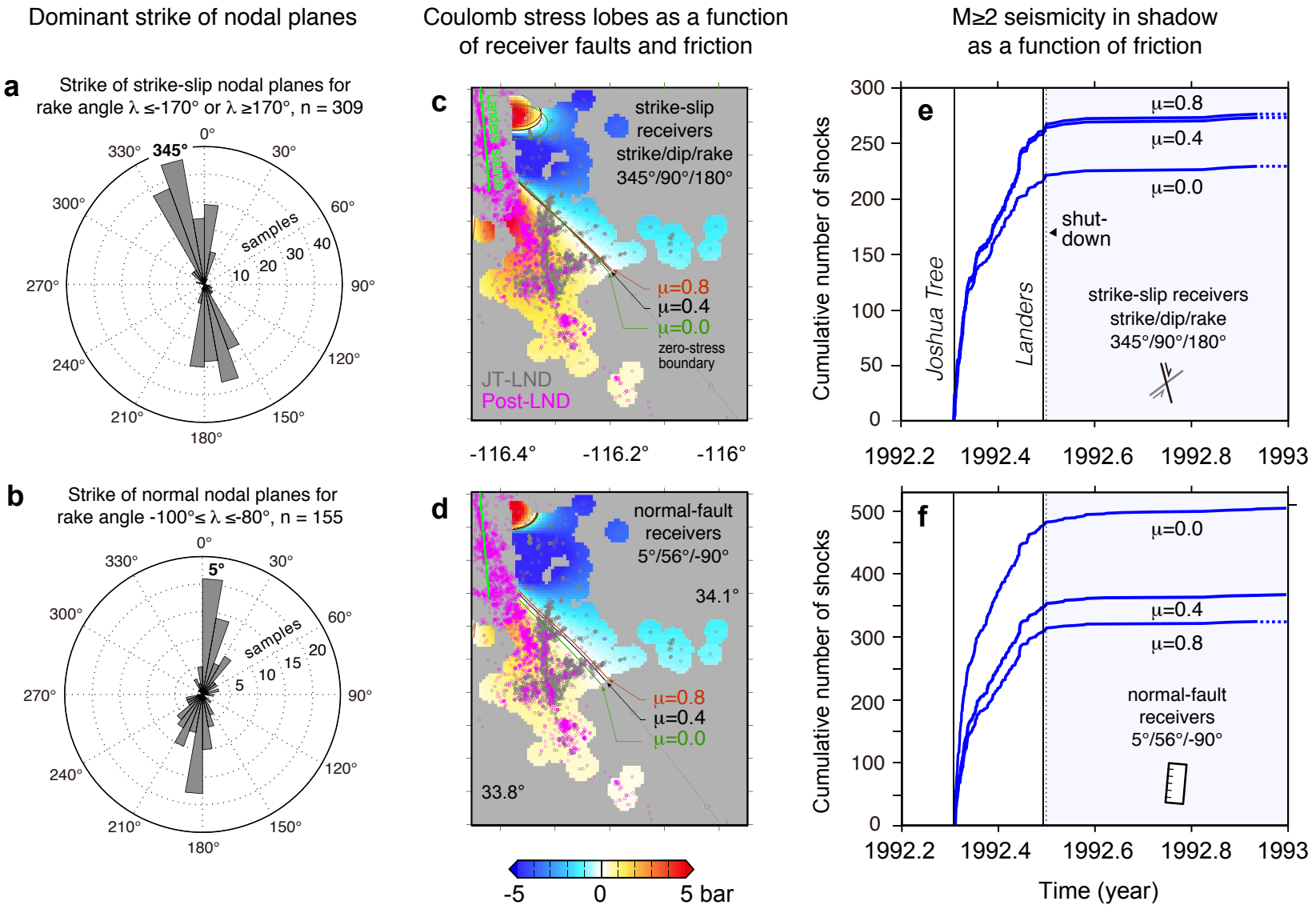

Supplementary Figure 4
NGS-2011-08-01314C
Toda et al.

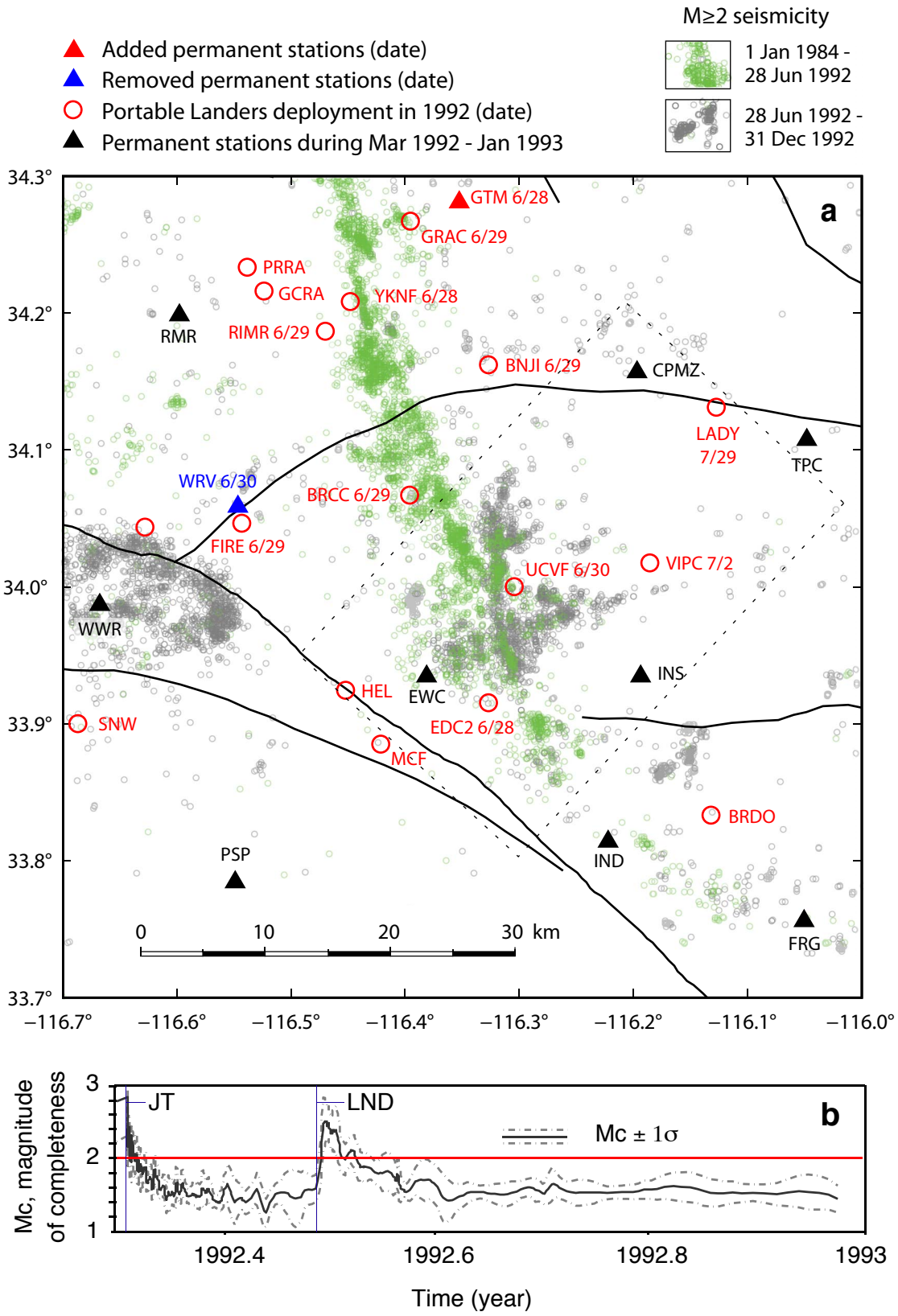

Supplementary Figure 5
NGS-2011-08-01314C
Toda et al.

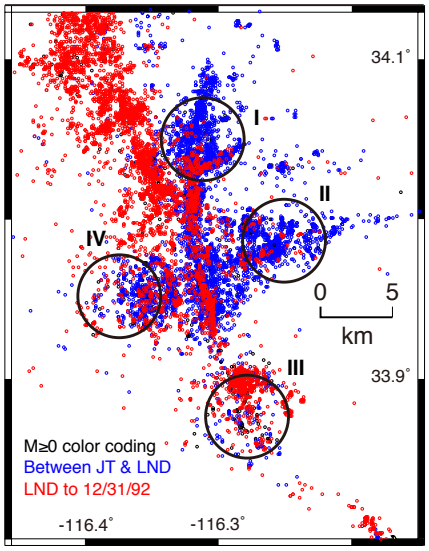

JT= Joshua Tree earthquake

LND = Landers earthquae

R=2.35 km

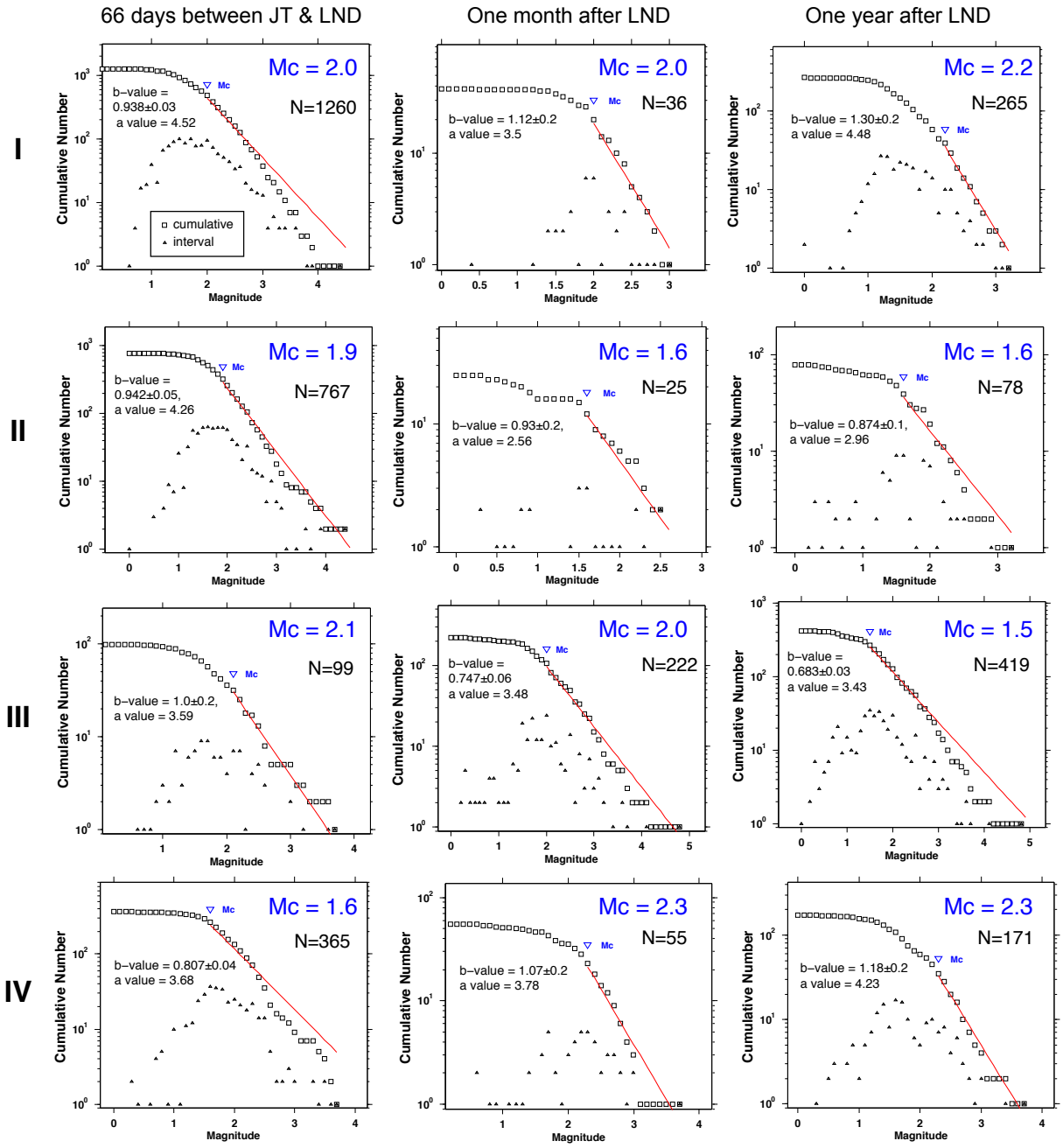

Supplementary Figure 6
NGS-2011-08-01314C
Toda et al.

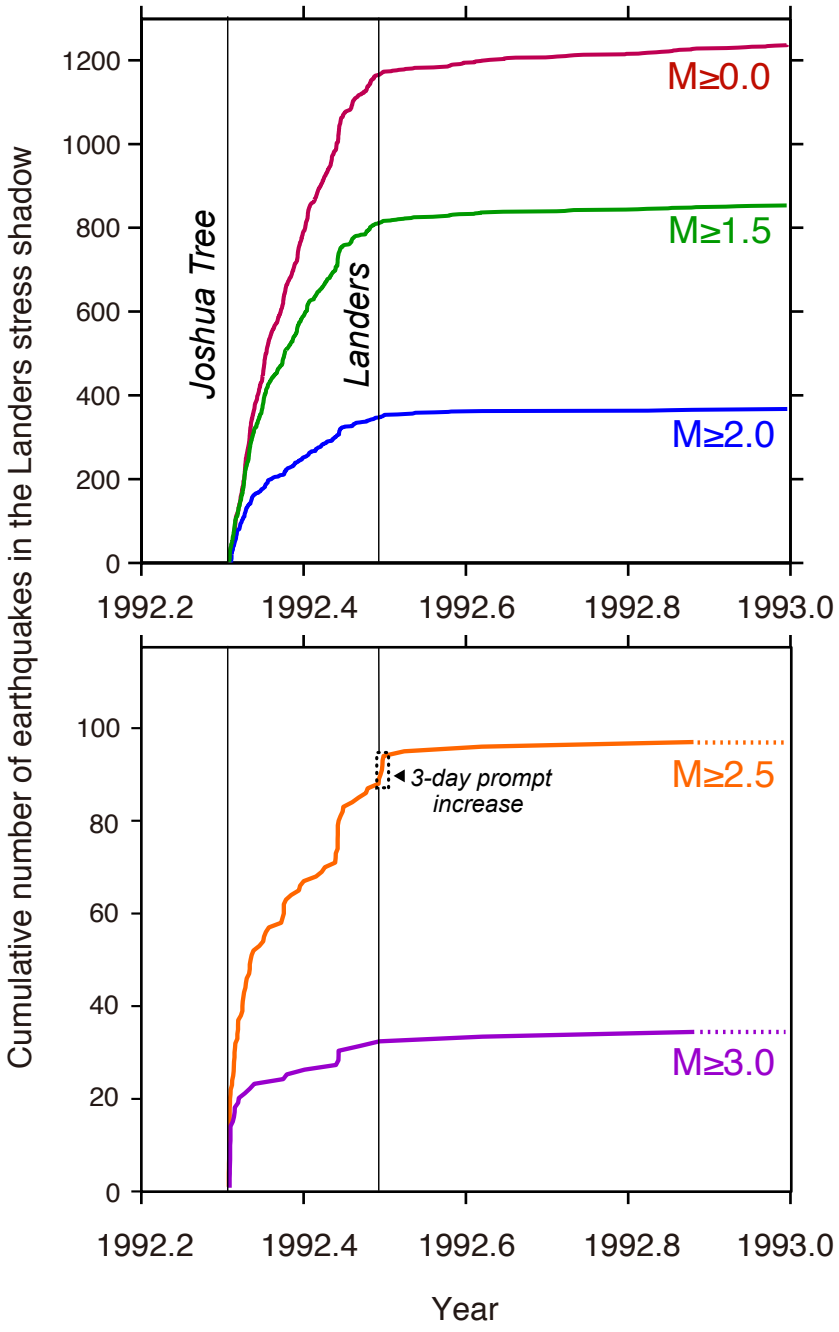

Supplementary Figure 7
NGS-2011-08-01314C
Toda et al.